Effects of Angular Frequency During Clinorotation on Mesenchymal Stem Cell Morphology and Migration

Original article, submitted on the 16th of March 2015 to
npj Microgravity

Carlos Luna, Ph.D.,[1] Alvin G. Yew, Ph.D.,[2] Adam H. Hsieh, Ph.D.,[1,3]

[1] Fischell Department of Bioengineering, University of Maryland, College Park, MD, USA
[2] NASA Goddard Space Flight Center, Greenbelt MD, USA
[3] Department of Orthopaedics, University of Maryland, Baltimore, MD, United States

Running title: Effects of angular frequency on hMSCs
Keywords: mesenchymal stem cells, clinorotation, morphology, migration

*Corresponding author: Dr. Adam H. Hsieh
Address: Jeong H Kim Engineering Building, Rm 3242
Fischell Department of Bioengineering
University of Maryland
College Park, MD, 20742
United States
Tel: 1-301-405-7397
Fax: 1-301-405-9953
e-mail: hsieh@umd.edu

ABSTRACT

Background/Objectives: Ground-based microgravity simulation can reproduce the apparent effects of weightlessness in spaceflight using clinostats that continuously reorient the gravity vector on a specimen, creating a time-averaged nullification of gravity. In this work, we investigated the effects of clinorotation speed on the morphology, cytoarchitecture, and migration behavior of human mesenchymal stem cells (hMSCs).

Methods: We compared cell responses at clinorotation speeds of 0, 30, 60, and 75 rpm over 8 hours in a recently developed lab-on-chip-based clinostat system. Time lapse light microscopy was used to visualize changes in cell morphology during and after cessation of clinorotation. Cytoarchitecture was assessed by actin and vinculin staining, and chemotaxis was examined using time lapse light microscopy of cells in NGF (100 ng/ml) gradients.

Results: Among clinorotated groups, cell area distributions indicated a greater inhibition of cell spreading with higher angular frequency ($p < 0.005$), though average cell area at 30 rpm after 8 hours became statistically similar to control ($p = 0.794$). Cells at 75rpm clinorotation remained viable and were able to re-spread after clinorotation. In chemotaxis chambers clinorotation did not alter migration patterns in elongated cells, but most clinorotated cells exhibited cell retraction, which strongly compromised motility.

Conclusions: These results indicate that hMSCs respond to clinorotation by adopting more rounded, less spread morphologies. The angular frequency-dependence suggests that a cell's ability to sense the changing gravity vector depends on the speed of perturbation. For migration studies, cells cultured in clinorotated chemotaxis chambers were generally less motile and exhibited retraction instead of migration.

INTRODUCTION

Intricate multi-scale interactions among cells, tissues, and organs fundamentally govern human health, which has evolved on Earth under a constant gravitational load of 1 g (9.8 m/s^2). The biological mechanisms underlying the role of gravity in human health remain poorly understood, but their elucidation is necessary for enabling long-term manned space exploration. Numerous studies, supported by the National Aeronautics and Space Administration (NASA) and other space agencies, have shown deleterious effects of space travel on the human body, such as accelerated bone loss[1, 2], muscle tissue degeneration[3], and others[4]. Importantly, these observations may have broader implications beyond spaceflight applications to provide a more detailed understanding of diseases on Earth. In particular the musculoskeletal system has historically been a focal point in space biology research, because of the strikingly adverse changes that occur in astronauts[5]. More recently, studies have begun to investigate mesenchymal stem cells (MSCs) for their roles in musculoskeletal lineage determination[6], bone repair[7] and tissue maintenance[8].

While the most relevant environment for performing microgravity research is in space, competition to use space-based facilities, like the International Space Station (ISS), is fierce and is further complicated by substantial time and resource investments[9]. As a result, lower-cost and logistically-simpler alternatives are attractive and include sounding rockets[10] and parabolic flights[11], or in-lab devices such as random positioning machines[12] and clinorotation devices (clinostats)[13] to simulate microgravity. The selection of a specific technique usually depends on accessibility, cost, experimental design, and research question. Clinostats are amongst the most accessible methods to simulate microgravity, and they allow researchers to study living cells using standard laboratory tissue culture supplies[14].

Clinorotation experiments have provided significant insight into the behavior of biological organisms in space. The technique was originally developed to study gravitropism in plant development, and has revealed that gravity serves a key role in statocyte function, which is believed to be directly involved in plant gravisensing and growth patterns[15]. In animal and human cells, clinorotation has been used to recreate experiments that would otherwise be challenging to perform in space, such as high resolution microscopy[16] and assessment of stem

cell differentiation[17]. Cellular changes in microgravity have been associated with disruptions in the cytoskeleton and, consequently, changes in cell morphology and behavior[18, 19].

Although clinorotation is a standard ground-based tool, previously reported studies on the effects of simulated microgravity in MSCs have yielded conflicting findings (Table 1). For instance, some researchers have shown that microgravity enhances proliferation[17], while others have demonstrated inhibition[20]. Chondrogenic differentiation has also been found to be either promoted[21] or suppressed[22]. Similar inconsistencies have also been highlighted in a recent review[23]. Some of these observed discrepancies could be due to differences in culture media formulation and cell source, but it is also possible that the choice of clinorotation parameters used for an experiment may substantially influence cell behavior.

A two-dimensional clinostat rotates a sample along the longitudinal axis to produce a time-averaged nullification of the gravity vector. Theoretically speaking, in order to simulate microgravity effectively, the period of rotation should be shorter than some time constant that governs the rate processes involved in the cellular gravisensing machinery that enable a cell to 'perceive' and respond to the changing trajectory of the gravity vector (Figure 1). For conventional clinostats, however, there are also practical considerations that limit the angular frequency of rotation[24]. Specifically, rotation speed must be adjusted to balance sedimentation forces, centrifugal and Coriolis effects, and Stokes' drag. Because of these constraints, the parameters of angular rotation depend on the particular design and implementation of each experimental system.

To minimize the effects of these extrinsic stimuli, we recently developed a lab-on-chip clinorotation device (clinochip) that confines adhered cells within a small region along the axis of rotation, limiting residual accelerations to levels below 10^{-5}g at different rotation speeds[25]. Moreover, the clinochip is amenable to time lapse microscopy, which enables us to characterize the kinetics of cell spreading, changes in morphology, and migration with minimal disruption to the simulated microgravity environment. In this study, we used this device to investigate how angular frequency affects human mesenchymal stem cell (hMSC) behavior. Based on the concept that there are specific rate processes that govern cellular gravisensing (Figure 1), we hypothesize that hMSCs would exhibit angular frequency-dependent responses. The results of this work demonstrate that hMSCs can in fact 'detect' differences in rotation speed in a manner

that causes heterogeneous population shifts toward more rounded morphologies and retraction of cell area. This could have significant implications on our basic understanding of stem cell regulation as well as on strategies that are being used in stem cell-based applications.

MATERIALS AND METHODS

Materials

Human mesenchymal stem cells were obtained from a commercial source (PT-2501, Lonza, Walkersville, MD), and confirmed to be mycoplasma-free. Clinochip fabrication required microscope slides (12-544-1, Fisher Scientific, Waltham, MA) and 0.254mm thick PDMS sheets (HT-6240, Rogers Corporation, Rogers, CT). Fluorescence visualization was performed for actin using 5% (w/v) Texas red phalloidin (Life Technologies, Gaithersburg, MD) and for focal adhesions using 1µg/ml fluorescein-conjugated anti-vinculin (MA1-34629, Life Technologies). Fibronectin (FN; 354008, BD Biosciences, San Jose, CA) was used to enable cell adhesion, and nerve growth factor (NGF; 7S-NGF, Life Technologies) was used for migration experiments. Calcein-AM and ethidium homodimer-1 (L-3224, Life Technologies) were used to perform cell viability assays.

Experimental setup

In general, we used a single experimental system for all of our experiments, as detailed previously[25]. Briefly, the system consists of a custom microscope-mounted gear system, driven by a computer controlled stepper motor that rotates a small slide holder[25]. This slide holder can accommodate various custom and commercially available lab-on-chip devices. A non-rotating slide holder enables having a static (standard gravity) control condition performed concurrently. The entire system is enclosed in an environmental chamber (Precision Plastics, Inc., Beltsville, MD) and installed on an Olympus IX-81 epi-fluorescence microscope (Center Valley, PA).

Cell morphology platform

A custom ‘clinochip’ device was used for visualizing cell spreading (i.e. changes in cell morphology over time), and fabricated according to our previously described protocol[25]. This clinochip consists of three layers comprising polydimethylsiloxane (PDMS) sandwiched between

two layers of glass. In brief, we used a high-resolution razor cutter (FC8000, Graphtec, Irvine, CA) to trim stock PDMS sheets. The sheet was cut to length and width dimensions of microscope slides and with a single 1 mm wide, 30 mm long channel at the center. A second microscope slide was used as the third layer. Prior to assembly, two 1 mm diameter holes had been made in the top slide using a sandblaster (6500, Airbrasive, Piscataway, NJ) in order to provide access to the channels. The three layers were energetically bonded using a high frequency corona treater (BD-20AC, Electrotechnic Products, Chicago, IL).

The clinochip was first sterilized for 20 minutes in a UV chamber. To promote cell attachment, the channel was then treated with 100 µg/mL FN for 1 hour and washed with PBS before use. Passage 3 (P3) and P4 hMSCs were seeded into clinochip channels and incubated at 37 ºC for 10 minutes to allow for cell attachment, followed by commencement of clinorotation.

Cell migration platform

Cell migration was analyzed using commercially available Ibidi Chemotaxis slides (µ-Slide Chemotaxis 2D, Ibidi, Munich, Germany). The slides fit perfectly in our clinorotation device and the 2 mm x 1 mm dimensions of the chamber are suitable for simulated microgravity since they constrain cells to a narrow region about the axis of rotation to minimize centrifugal effects. First, a 100µg/mL FN solution was injected into the viewing chamber and incubated for 1 hour, followed by three PBS washes. Then, P3 and P4 hMSCs were plated and incubated at 37 ºC for 12 hours of initial seeding time. Our pilot experiments showed that after 12 hours the spreading areas of hMSCs reach a plateau so that cell spreading would not confound the cell migration data. As a first step, we chose to study hMSC chemotaxis mediated by NGF, one of several growth factors identified in this active field of research[26]. MSCs have been shown to express receptors to neurotrophic factors including NGF[27], and also secrete NGF during tissue repair[28]. In these migration experiments, NGF was prepared as a 100 ng/ml solution and injected into the top ports of the chamber. Following manufacturer's instructions, the same volume was aspirated from the opposite port in order to create a chemical gradient.

Clinorotation and time-lapse imaging

Both morphology and chemotaxis platforms were rotated along the axis of the channels in which cells were cultured. Residual accelerations are one to two orders of magnitude smaller than

conventional clinostats, even at 75 rpm[25]. Before the experiment, we made sure that the channels did not contain any bubbles, in order to minimize any other external effects such as shear stress and dehydration. During imaging, we constrained our analyses to cells near the axis of rotation, away from the sides of the channel, in order to avoid potential edge effects.

At the appropriate times (10 min after seeding for morphology assays; 12 hrs after seeding for chemotaxis and migration assays to allow the cells to become fully spread), clinorotation was initiated at 30, 60, or 75 rpm and maintained over the course of 8 hours. Clinochips at 0 rpm (non-rotated) were used as a control (standard gravity). During each hour, rotation was paused for a total of 60 seconds, and a set of bright field images of the clinochip were acquired at 200x magnification. At the end of the 8 hour period, cells were fixed in 4% paraformaldehyde, and fluorescently stained for actin and vinculin. Captured images were analyzed using ImageJ (NIH).

Cell viability and recovery after clinorotation

Cell viability was determined using calcein-AM (green) to indicate intracellular esterase activity for live cells and ethidium homodimer-1 (red) to indicate loss of plasma membrane integrity for dead cells. Calcein (final concentration 4μM) and ethidium homodimer (final concentration 2μM) were added to cell culture media that was used to plate hMSCs in FN-treated clinochips. After 10 minutes of attachment, clinochips were either rotated at 75 rpm or maintained at standard gravity conditions (non-rotated control) and fluorescence micrographs were taken at 1, 4, and 8 hours during clinorotation.

In addition to the live/dead assays, we acquired light micrographs of cell morphology in standard gravity following exposure to (a) 1 or 4 hrs of 30rpm clinorotation, (b) 1 or 4 hrs of 60rpm clinorotation, or (c) 1, 4, or 8 hrs of 75 rpm clinorotation. After termination of the clinorotation treatment, images were acquired in standard gravity every 30 min for 4 hours, and then analyzed for cell area and shape factor using ImageJ (NIH).

Statistical analyses

Because no prior publications have quantified cell areas during clinorotation, we relied on pilot data for descriptive statistics to make sample size calculations. Assuming a critical significance level of $\alpha = 0.05$, statistical power of 0.9 ($\beta = 0.1$), and a detectable difference equal to the population standard deviation, we performed a power analysis to calculate an estimated sample

size of n=23, according to Sokal and Rohlf[29]. To ensure adequate statistical power for cell area measurements, we chose to include at least n=30 for each sample group (Table 2), acquired over several experimental replicates. All data are expressed as mean ± standard error of the mean. Variance did not markedly differ between groups (less than four-fold). Average cell areas among different clinorotation speeds were first log transformed to improve normality. Differences between clinorotation groups were then statistically analyzed using the Welch's t test for samples with unequal variance and unequal sample size, with Tukey *post hoc* tests for multiple pairwise comparisons.

We analyzed the difference in cell velocity and directionality between 0 (n = 15) and 75 rpm (n = 6) with only cells that were actively migrating using the Welch's t test for samples with unequal variance and sample size. Similarly, we analyzed the difference between retracting cells for 30 and 75 rpm (at 0, 1, 2, 3 and 4 hours) with only areas from cells that were actively retracting (n = 28) using the Welch's t test, with Tukey *post hoc* test for multiple pairwise comparison.

RESULTS

Simulated microgravity affects cell spreading

Simulated microgravity had a profound effect on both the extent and kinetics of cell spreading (Figure 2). After the initial 10 minute cell attachment and before rotation commenced, all of the groups possessed similar cell areas of approximately 500 μm^2. We found that hMSCs in the non-rotated 0 rpm condition (i.e. standard gravity) markedly increased spreading areas within 1 hour after plating, reaching an average of 2000 μm^2. Their spreading area increased gradually with time, until they reached an average of 3000 μm^2 by 8 hours. For clinorotated groups, cell spreading was impeded almost immediately. At 1 hour, cells in the 30 rpm group were significantly smaller than control with an average cell area slightly above 1000 μm^2; cells at 60 and 75 rpm were both significantly different from 0 and 30 rpm, remaining rounded and small. The effects of clinorotation continued to affect cell spreading over the course of the entire 8 hour experiment in a rotation speed-dependent manner. By 8 hours, we measured a statistically similar but smaller average area of 2750 μm^2 for cells at 30 rpm. In contrast, the 60 rpm group had an

average area of 2192 μm^2, and the 75 rpm group had the lowest cell area of 1500 μm^2, both statistically smaller than 0 and 30 rpm.

From a kinetics perspective, the time required for cell spreading areas to reach 2000 μm^2 was within 1 hour for non-rotating controls, within 4 hours for 30 rpm, and within 8 hours for 60 rpm. Our experiments did not run long enough to determine whether or not cells would reach this mark for the 75 rpm condition, but based on the observed trends, it appears that cell spreading no longer increases after 7 hours. These results indicate that cell spreading is markedly affected by angular frequency and that these effects can be observed as soon as 1 hour after clinorotation starts. Finer temporal resolutions and longer durations in future experiments may provide more detailed insight on the time constant of important cellular processes associated with cellular gravisensing.

One notable observation we made was that cells within each clinorotation speed were not uniformly spread. Since individual cells did not accurately represent the population characteristics, we plotted the group-wise distributions of cell morphologies at various time points (Supplementary Figure 1). The 0 rpm control group adopts a broad distribution of cell areas within the first hour, followed by the 30 and 60 rpm groups. By 8 hours, it is clear that the 0, 30, and 60 rpm cell populations encompassed comparable ranges of cell areas. The 75 rpm group, however, exhibited a much more narrow distribution. Likewise, when staining for filamentous actin we found that cells also spanned a range of cell shapes within each group (Supplemental Figure 2). There were no discernable differences in actin organization between cells of *similar morphology* (elongated or rounded), even when comparing across *different clinorotation conditions.* This suggests that the observed population differences with angular frequency is caused by disparate effects on individual cells, perhaps by triggering/overcoming some intrinsic signal within cells to reduce cell adhesion, suppress actin stress fiber formation, and consequently induce cell rounding. It is unclear whether simulated microgravity directly affects actin stress fiber assembly to result in cell rounding, or whether cell rounding induced by simulated microgravity is what inhibits stress fiber formation.

To quantify these differences in cell shape as a function of clinorotation speed, we computed circularity ($Circularity = 4\pi * Area/Perimeter^2$) since it accommodates more abstract shapes than an aspect ratio calculation. We assigned circularity values above 0.6 to cells that

were considered rounded (Figure 3, black), values between 0.3 and 0.6 to semi-elongated cells (Figure 3, hatch) and values below 0.3 to elongated cells (Figure 3, gray). As expected from the previous area measurements, Figure 3 clearly shows that increasing clinorotation speed results in a larger percentage of rounded cells in its population. The number of elongated cells was significantly reduced with increasing clinorotation speed, and no elongated cells were found at 75 rpm.

Plotting cell circularity against cell area for each clinorotation speed at different time points, we clearly see a temporal increase in area associated with cell elongation in 0 rpm control cells (Supplemental Figure 3). This trend becomes disrupted with exposure to 30 and 60 rpm clinorotation, as cells tended to exhibit a broad range of circularity and area. However, only at 75 rpm does the cell population maintain high circularity and smaller areas across time points (1, 4 and 8 hours). Overall, our morphology analysis demonstrates that the cell population at 75 rpm possesses a more consistent morphology (average area, cell distribution, circularity vs. area over time) over time.

Cell viability and recovery after clinorotation

To determine whether there was any loss of viability or if rounded cells were undergoing apoptosis, we exposed cells to 75 rpm and used a live/dead assay after 1, 4 and 8 hours of clinorotation (Figure 4). We found no difference in cell viability or changes in cell number when compared to control; in fact, the majority of cells were alive (>90%). Under light microscopy, we observed no evidence of apoptosis (i.e. membrane blebbing) for the cells that were not viable. This also indicates that our clinochip system can be used effectively without loss of cells due to lifting or cell death for at least 8 hours.

We investigated whether clinorotation effects on cell morphology are reversible by performing time lapse microscopy after exposure to 1, 4, and 8 hours of 75 rpm clinorotation. Following cessation of clinorotation, all cells increased their areas and round cells became more elongated, similar to most of the cells in standard gravity controls (Figure 4). Similar experiments were also repeated for 30 and 60 rpm after 1 and 4 hours of clinorotation (Supplemental Figure 4).

Simulated microgravity inhibits cell migration by inducing cell rounding

For cell migration experiments, cells were seeded in Ibidi chemotaxis chips with a chemical gradient of 100 ng/ml NGF to promote cell migration. Under clinorotation, only a few cells migrated while most cells did not (see Table 2 for cell numbers). Cells that were actively migrating at 75 rpm had a similar velocity ($p = 0.391$) and directionality ($p = 0.822$) when compared to control cells (Figure 5). Cells that were not migrating under simulated microgravity exhibited morphological retraction (Figure 5). In other words, cell areas changed from fully-spread morphologies to more rounded ones. These observations complement what we observed in our cell spreading experiments, even when the initial conditions were different (10 min for spreading assays vs. 12 hours for chemotaxis and migration assays). We found that during clinorotation cells retracted their area, but did so independently of rotation speed ('0 hr' $p = 0.539$, '1 hr' $p = 0.288$, '2 hrs' $p = 0.963$, '3 hrs' $p = 0.848$, '4 hrs' $p = 0.689$, between 30 and 75 rpm). After 4 hours of clinorotation during chemotaxis, cells at 30 and 75 rpm reached an average area of 2500 μm^2, which is a value similar to the spreading experiments for 30 rpm at 8 hours ($p = 0.962$ between 30 rpm, $p = 0.975$ between 75 rpm). However, we did not conduct experiments long enough to determine steady state retracted cell areas.

Our results indicate that the cellular response to simulated microgravity is more dominant than chemotactic signals, suggesting the role of migration of hMSCs to tissue repair sites might be suppressed in microgravity. We base this conclusion on our observations of response to NGF at a concentration of 100 ng/ml. However, these results were obtained with only one concentration of NGF and it is possible that different concentrations or other chemotactic molecules can elicit a stronger chemotactic response. For example stromal derived factor-1, which is known to be a strong homing signal for hMSCs[30]. Nevertheless, because the response of adhered cells to clinorotation is retraction of cellular processes, we believe that the behavior will be similar, unless the chemotactic agent can also enhance cell adhesion.

DISCUSSION

Understanding how angular frequency, or rotation speed, of clinorotation affects cell behavior is a critical aspect of microgravity simulation experiments, so that the role of the changing gravity vector in cellular regulation can be appropriately considered. In this work we show that hMSCs

can behave differently depending on clinorotation speed. In particular, while average cell area increased more slowly at 30 rpm compared with non-rotated controls, it continues along an upward trajectory at 8 hours and seems to be converging with control values. For higher rotational speeds, cell area increases even more slowly, and appears to reach a plateau by 8 hours at 75 rpm. This suggests changes in cell morphology may approach a limit at an angular frequency that is close to 75 rpm, and almost certainly must exceed 30 rpm. While these results are relevant to our clinochip configuration, results may vary for other clinostat devices, particularly for those that support cells in suspension.

Our results are consistent with other research showing that rotation speed affects animal cells, plants, and bacteria (E. coli). For example, a study on osteoblastic ROS 17/2.8 cells reported that rotations at 10 and 40 rpm did not exhibit reproducible, detectable changes from stationary control cells[31]. Only a speed of 50 rpm showed reproducible changes in actin cytoskeleton and cell surface integrin β1 and apoptosis. The same effect has been observed with E. coli[32], which exhibited differential response as a function of clinorotation speeds from 10 to 50 rpm. Interestingly, the difference between 40 and 50 rpm is only 0.1674 of a cycle per second, indicating that cells can be highly sensitive to small changes in angular frequency.

Although a precise gravisensing mechanism has yet to be determined, it must be one that can detect subtle alterations to external forces in a short period of time. Our data indicate that it is linked to pathways that are involved in cell spreading and cytoskeletal organization, two phenomena that have been observed for different cell types. Potential candidates could be one or more molecules already known to play important roles in cellular mechanoregulation, such as the Rho family of GTPases[33], ion mechanosensitive channels[34], intracellular calcium[35], nuclear deformations[36], focal adhesions, or other cell surface receptors[37]. Although mechanosensitive pathways seem the most direct apparatus for gravisensing, others have also suggested the importance of external environmental factors including fluid shear, fluid and nutrient exchange, oxygen content, buoyancy, and changes in the extracellular matrix[38]. Thus, clinostats used to probe candidate gravisensing receptors should minimize external environmental variables that arise from clinostat operation.

In the context of a proposed framework for cellular gravisensing, the current results are consistent with our working hypothetical model. Standard gravity would constitute a constant

gravitational stimulus and be detectable to all cells. With intermediate timescales of gravitational nullification, the probability for a single cycle of rotational perturbation to evade gravisensing in each cell would assume a broad distribution. Since any putative biochemical gravisensing reaction(s) would be stochastic, the probability for gravisensory evasion in each cell would decrease with both lower angular frequency and exposure to longer duration perturbations. We did in fact observe such trends, as a result of the time lapse, single cell measurement capabilities of the clinochip system.

For our clinochips, we do not expect that centripetal forces play a role with our observed angular frequency-dependence, since residual accelerations were calculated to be on the micro scale regime. In addition, because the capillary number (indicative of viscous forces) is orders of magnitude smaller than surface tension, fluid shear forces are deemed negligible. There is also no enhanced nutrient transport that accompanies clinorotation in our system. Without these confounding factors, it seems reasonable to conclude that the cell morphology differences we observed were due to changes in the angular frequency of clinorotation.

We believe the rounding and retracted cell area of hMSCs in simulated microgravity inhibit migration in the presence of a chemical gradient. Interestingly, the kinetics of cell area changes during retraction were different from those during spreading, and were also angular frequency-independent, suggesting that distinct gravisensing mechanisms may regulate different processes. Similarly, other cell processes, and even cell fate, could be affected[39]. In the same way that microgravity may produce these cellular alterations, other mechanical stimuli and substrate characteristics can also modulate cell function[40].

Stem cell morphology has a strong correlation with cellular phenotype and differentiation potential [41, 42]. It has been demonstrated in prior work that spread cells have a higher tendency to undergo osteogenesis and that cells with rounded morphologies are more susceptible to adipogenesis [42]. Because of the short-term nature of this current study, it is not possible to establish whether hMSCs in our system would behave according to these trends. However, our data would suggest that cells at 30 rpm clinorotation would be more amenable to osteogenic differentiation while cells at 75 rpm would tend toward adipogenic or chondrogenic lineages. This may help explain the conflicting reports on MSC differentiation during clinorotation that we and others[23] have observed. Future longer-term studies with the clinochip are required to

explore hMSC differentiation potential. Specifically, since we have shown that the population distribution of cell morphologies can be controlled by the angular frequency of rotation, we may be able to derive cellular phenotypes desirable for stem cell renewal, repair, and tissue engineering.

Contributions. C.L, A.Y, A. H conceived the project and analyzed the data, C.L. performed the experiments, A.Y. developed the lab-on-chip clinostat, and all authors contributed to the writing.

Competing Interests. The authors (Drs. Luna, Yew and Hsieh) have no competing interests in relation to the work described.

Funding. This work was supported by NASA Space Biology Program, Grant NNX13AM06G.

REFERENCES

1. Zwart SR, Morgan JL, Smith SM. Iron status and its relations with oxidative damage and bone loss during long-duration space flight on the International Space Station. The American journal of clinical nutrition. 2013;98(1):217-23.

2. LeBlanc A, Schneider V, Shackelford L, West S, Oganov V, Bakulin A, et al. Bone mineral and lean tissue loss after long duration space flight. Journal of musculoskeletal & neuronal interactions. 2000;1(2):157-60.

3. Fitts RH, Trappe SW, Costill DL, Gallagher PM, Creer AC, Colloton PA, et al. Prolonged space flight-induced alterations in the structure and function of human skeletal muscle fibres. The Journal of physiology. 2010;588(Pt 18):3567-92.

4. Whitson PA, Pietrzyk RA, Jones JA, Nelman-Gonzalez M, Hudson EK, Sams CF. Effect of potassium citrate therapy on the risk of renal stone formation during spaceflight. The Journal of urology. 2009;182(5):2490-6.

5. Morey ER, Baylink DJ. Inhibition of bone formation during space flight. Science. 1978;201(4361):1138-41.

6. Pittenger MF, Mackay AM, Beck SC, Jaiswal RK, Douglas R, Mosca JD, et al. Multilineage potential of adult human mesenchymal stem cells. Science. 1999;284(5411):143-7.

7. Bruder SP, Fink DJ, Caplan AI. Mesenchymal stem cells in bone development, bone repair, and skeletal regeneration therapy. Journal of cellular biochemistry. 1994;56(3):283-94.

8. Caplan AI, Dennis JE. Mesenchymal stem cells as trophic mediators. Journal of cellular biochemistry. 2006;98(5):1076-84.

9. Luttges MW. Recognizing and optimizing flight opportunities with hardware and life sciences limitations. Transactions of the Kansas Academy of Science Kansas Academy of Science. 1992;95(1-2):76-86.

10. Huijser R, Aartman L, Willemsen H. Cells in Space - Sounding Rocket Facilities for Cell Biology and Biotechnology in Microgravity. Esa Sp Publ. 1990;307:455-66.

11. Paul AL, Manak MS, Mayfield JD, Reyes MF, Gurley WB, Ferl RJ. Parabolic flight induces changes in gene expression patterns in Arabidopsis thaliana. Astrobiology. 2011;11(8):743-58.

12. van Loon JJWA. Some history and use of the random positioning machine, RPM, in gravity related research. Advances in Space Research. 2007;39(7):1161-5.

13. Hemmersbach R, Strauch SM, Seibt D, Schuber M. Comparative studies on gravisensitive protists on ground (2D and 3D clinostats) and in microgravity. Microgravity Sci Tec. 2006;18(3-4):257-9.

14. Klaus DM. Clinostats and bioreactors. Gravitational and space biology bulletin : publication of the American Society for Gravitational and Space Biology. 2001;14(2):55-64.

15. Lorenzi G, Perbal G. Root-Growth and Statocyte Polarity in Lentil Seedling Roots Grown in Microgravity or on a Slowly Rotating Clinostat. Physiologia plantarum. 1990;78(4):532-7.

16. Toy MF, Richard S, Kuhn J, Franco-Obregon A, Egli M, Depeursinge C. Enhanced robustness digital holographic microscopy for demanding environment of space biology. Biomedical optics express. 2012;3(2):313-26.

17. Yuge L, Kajiume T, Tahara H, Kawahara Y, Umeda C, Yoshimoto R, et al. Microgravity potentiates stem cell proliferation while sustaining the capability of differentiation. Stem cells and development. 2006;15(6):921-9.

18. Buravkova LB, Romanov YA. The role of cytoskeleton in cell changes under condition of simulated microgravity. Acta astronautica. 2001;48(5-12):647-50.

19. Higashibata A, Imamizo-Sato M, Seki M, Yamazaki T, Ishioka N. Influence of simulated microgravity on the activation of the small GTPase Rho involved in cytoskeletal formation--molecular cloning and sequencing of bovine leukemia-associated guanine nucleotide exchange factor. BMC biochemistry. 2006;7:19.

20. Dai ZQ, Wang R, Ling SK, Wan YM, Li YH. Simulated microgravity inhibits the proliferation and osteogenesis of rat bone marrow mesenchymal stem cells. Cell proliferation. 2007;40(5):671-84.

21. Yu B, Yu D, Cao L, Zhao X, Long T, Liu G, et al. Simulated microgravity using a rotary cell culture system promotes chondrogenesis of human adipose-derived mesenchymal stem cells via the p38 MAPK pathway. Biochemical and biophysical research communications. 2011;414(2):412-8.

22. Sheyn D, Pelled G, Netanely D, Domany E, Gazit D. The effect of simulated microgravity on human mesenchymal stem cells cultured in an osteogenic differentiation system: a bioinformatics study. Tissue engineering Part A. 2010;16(11):3403-12.

23. Ulbrich C, Wehland M, Pietsch J, Aleshcheva G, Wise P, van Loon J, et al. The impact of simulated and real microgravity on bone cells and mesenchymal stem cells. BioMed research international. 2014;2014:928507.

24. Klaus DM, Todd P, Schatz A. Functional weightlessness during clinorotation of cell suspensions. Adv Space Res. 1998;21(8-9):1315-8.

25. Yew AG, Atencia J, Hsieh AH. Lab-on-Chip Clinorotation System for Live-Cell Microscopy Under Simulated Microgravity. Cell Mol Bioeng. 2014;7(1):165-70.

26. Ozaki Y, Nishimura M, Sekiya K, Suehiro F, Kanawa M, Nikawa H, et al. Comprehensive analysis of chemotactic factors for bone marrow mesenchymal stem cells. Stem cells and development. 2007;16(1):119-29.

27. Quirici N, Soligo D, Bossolasco P, Servida F, Lumini C, Deliliers GL. Isolation of bone marrow mesenchymal stem cells by anti-nerve growth factor receptor antibodies. Exp Hematol. 2002;30(7):783-91.

28. Wakabayashi K, Nagai A, Sheikh AM, Shiota Y, Narantuya D, Watanabe T, et al. Transplantation of human mesenchymal stem cells promotes functional improvement and increased expression of

neurotrophic factors in a rat focal cerebral ischemia model. Journal of neuroscience research. 2010;88(5):1017-25.

29. Sokal RR, Rohlf FJ. Single classification analysis of variance: finding the sample size required for a test. Biometry. 3rd ed. ed. New York City, NY: W. H. Freeman and Co.; 1995. p. 260-5.

30. Son BR, Marquez-Curtis LA, Kucia M, Wysoczynski M, Turner AR, Ratajczak J, et al. Migration of bone marrow and cord blood mesenchymal stem cells in vitro is regulated by stromal-derived factor-1-CXCR4 and hepatocyte growth factor-c-met axes and involves matrix metalloproteinases. Stem cells. 2006;24(5):1254-64.

31. Sarkar D, Nagaya T, Koga K, Nomura Y, Gruener R, Seo H. Culture in vector-averaged gravity under clinostat rotation results in apoptosis of osteoblastic ROS 17/2.8 cells. Journal of bone and mineral research : the official journal of the American Society for Bone and Mineral Research. 2000;15(3):489-98.

32. Baker PW, Meyer ML, Leff LG. Escherichia coli growth under modeled reduced gravity. Microgravity Sci Technol. 2004;15(4):39-44.

33. Louis F, Deroanne C, Nusgens B, Vico L, Guignandon A. RhoGTPases as Key Players in Mammalian Cell Adaptation to Microgravity. BioMed research international. 2015;2015:747693.

34. Sun Z, Cao X, Zhang Z, Hu Z, Zhang L, Wang H, et al. Simulated microgravity inhibits L-type calcium channel currents partially by the up-regulation of miR-103 in MC3T3-E1 osteoblasts. Scientific reports. 2015;5:8077.

35. Kohn FPM. High Throughput Fluorescent Screening of Membrane Potential and Intracellular Calcium Concentration Under Variable Gravity Conditions. Microgravity Sci Tec. 2013;25(2):113-20.

36. Ng TL, Gown AM, Barry TS, Cheang MC, Chan AK, Turbin DA, et al. Nuclear beta-catenin in mesenchymal tumors. Modern pathology : an official journal of the United States and Canadian Academy of Pathology, Inc. 2005;18(1):68-74.

37. Li J, Zhang S, Chen J, Du T, Wang Y, Wang Z. Modeled microgravity causes changes in the cytoskeleton and focal adhesions, and decreases in migration in malignant human MCF-7 cells. Protoplasma. 2009;238(1-4):23-33.

38. Hammond TG, Hammond JM. Optimized suspension culture: the rotating-wall vessel. American journal of physiology Renal physiology. 2001;281(1):F12-25.

39. Matsuoka F, Takeuchi I, Agata H, Kagami H, Shiono H, Kiyota Y, et al. Morphology-based prediction of osteogenic differentiation potential of human mesenchymal stem cells. PloS one. 2013;8(2):e55082.

40. Maul TM, Chew DW, Nieponice A, Vorp DA. Mechanical stimuli differentially control stem cell behavior: morphology, proliferation, and differentiation. Biomechanics and modeling in mechanobiology. 2011;10(6):939-53.

41. Kilian KA, Bugarija B, Lahn BT, Mrksich M. Geometric cues for directing the differentiation of mesenchymal stem cells. Proc Natl Acad Sci U S A. 2010;107(11):4872-7.

42. McBeath R, Pirone DM, Nelson CM, Bhadriraju K, Chen CS. Cell shape, cytoskeletal tension, and RhoA regulate stem cell lineage commitment. Developmental cell. 2004;6(4):483-95.

43. Nishikawa M, Ohgushi H, Tamai N, Osuga K, Uemura M, Yoshikawa H, et al. The effect of simulated microgravity by three-dimensional clinostat on bone tissue engineering. Cell transplantation. 2005;14(10):829-35.

44. Wu X, Li SH, Lou LM, Chen ZR. The effect of the microgravity rotating culture system on the chondrogenic differentiation of bone marrow mesenchymal stem cells. Molecular biotechnology. 2013;54(2):331-6.

45. Zhang X, Nan Y, Wang H, Chen J, Wang N, Xie J, et al. Model microgravity enhances endothelium differentiation of mesenchymal stem cells. Die Naturwissenschaften. 2013;100(2):125-33.

46. Uddin SM, Qin YX. Enhancement of osteogenic differentiation and proliferation in human mesenchymal stem cells by a modified low intensity ultrasound stimulation under simulated microgravity. PloS one. 2013;8(9):e73914.

47. Zayzafoon M, Gathings WE, McDonald JM. Modeled microgravity inhibits osteogenic differentiation of human mesenchymal stem cells and increases adipogenesis. Endocrinology. 2004;145(5):2421-32.

48. Saxena R, Pan G, McDonald JM. Osteoblast and osteoclast differentiation in modeled microgravity. Annals of the New York Academy of Sciences. 2007;1116:494-8.

49. Meyers VE, Zayzafoon M, Gonda SR, Gathings WE, McDonald JM. Modeled microgravity disrupts collagen I/integrin signaling during osteoblastic differentiation of human mesenchymal stem cells. Journal of cellular biochemistry. 2004;93(4):697-707.

50. Chen J, Liu RR, Yang Y, Li J, Zhang XF, Li JC, et al. The simulated microgravity enhances the differentiation of mesenchymal stem cells into neurons. Neurosci Lett. 2011;505(2):171-5.

Figure Legend

Figure 1. Perceived gravity biases for cell events under clinorotation. In the cell-fixed frame of reference, the magnitude of the gravity vector oscillates in a sinusoidal fashion during clinorotation. Lightly shaded blocks illustrate hypothetical time constants required for various intrinsic cellular events to occur. The total gravity forces experienced by cells are shaded in darker colors to help clarify the idea that slower clinorotation (Top) may fail to nullify gravity biases for some cell events, while faster clinorotation (Bottom) could provide better nullification.

Figure 2. Human mesenchymal stem cell spreading areas in simulated microgravity. a) Time analysis of cell spreading of hMSCs in simulated microgravity at different rotation speeds (0, 30, 60 and 75 rpm). Note that increasing the rotation speed resulted in less spreading area over time. NS Indicates statistically similar average areas ($p > 0.05$). b) Representative micrographs of hMSCs spreading in a glass substrate coated with FN at different rotation speeds for 8 hours (0, 30, 60 and 75 rpm). Note that cells at a speed of 30 rpm were more similar to control, while cells at 60 and 75 rpm have adopted a more rounded morphology.

Figure 3. Human mesenchymal stem cell shape as function of time at different rotation speeds. We analyzed the shapes of hMSCs at different rotation speeds as a function of time for 1, 4 and 8 hours; black = rounded cells, line pattern = semi-elongated cells, gray = elongated. Cells were stained with phalloidin (actin, red) and representative micrographs were selected for each morphological configuration. At 0 rpm, cells were rounded at the first hour and were mostly elongated at the end of our time-lapse. At 30 rpm, the number of elongated cells was reduced but still present at 4 and 8 hours. At 60 rpm, there were no elongated cells at 4 hours and there were mostly semi-elongated cells at 8 hours. At 75 rpm, the number of rounded cells increases at every time point.

Figure 4. Cell viability and recovery after clinorotation. Cell spreading dynamics were measured for cells after 1, 4, and 8 hours of clinorotation at 75 rpm. Four hours after clinorotation was terminated, cell areas were observed to increase by a factor of 1.4-1.8 times. (Bottom) Time-lapse micrographs illustrate a round cell adopting a more elongated morphology during recovery in standard microgravity. A Live/Dead stain was used to analyze both cells in the control and cells exposed to clinorotation, and revealed that cell viability was preserved over

time. A fluorescence micrograph for live cells (green) and dead cells (red) is provided to demonstrate the data we analyzed.

Figure 5. Analysis of chemotactic cell migration in simulated microgravity. Human mesenchymal stem cell spreading in simulated microgravity. Cells stimulated by a chemotactic signal (NGF) in microgravity exhibited two types of behavior: Cells that were actively migrating, had a similar velocity ($p = 0.391$) and directionality ($p = 0.822$) in simulated microgravity and in non-rotated conditions. However, most cells in simulated microgravity did not exhibit active migration (see red arrow, N = 17 cells retracting, N = 6 cells migrating). Cells that were not migrating retracted their area as a function of time. This behavior was similar at different rotation speeds ($p = 0.698$ at 4 hrs between 30 and 75 rpm). These results indicate that the morphological response to microgravity is stronger than the response to chemotaxis and migration.

Supplemental Figure 1. Histograms of cell populations, binned by area, at different time points. We analyzed the changes in cellular distribution based on cell area for different clinorotation speeds at 1, 4 and 8 hours. Cell distribution at 1 hour, note that 60 rpm and 75 rpm have very similar cell distributions, while 30 and 0 rpm have larger areas. Cell distributions at 4 hours, the difference in cell areas increases between all rotation speeds. Cell distributions at 8 hours, note that cells at 75 rpm remained the less spread during our analysis, which indicates the existence of a rotation speed threshold for cells to maintain their microgravity morphology. Dashed lines indicate Weibull regression fits to each histogram. Data above 3500 μm^2 are not shown for the purpose of clarity.

Supplemental Figure 2. Representative cells found in experiments with fluorescence staining for actin filaments and focal adhesions at different rotation speeds. We stained cells with Texas-red phalloidin (actin) and anti-vinculin (green) for focal adhesions. We observed that at every clinorotation speeds there were cells rounded and cells that were spread. Cells that were rounded possessed mostly cortical actin staining, while cells that were spread had actin stress fibers independent of clinorotation speed. All cells that were spread had focal adhesions at every clinorotation speed. These results indicate that the response to microgravity varies from cell to cell.

Supplemental Figure 3. Human mesenchymal stem cell area as a function of shape. Distribution of hMSCs as a function of area vs. circularity shows that under standard gravity, cell area and morphology increase over time. When subjected to microgravity, the rotation of speed is proportional to the number of circular cells. In our specific system, a speed of 75 rpm shows the most consistent cell behavior, with most circular cells at every time point.

Supplemental Figure 4. Cell spreading dynamics after clinorotation. Cells were subjected to clinorotation at 30, 60 and 75 rpm. The recovery after clinorotation for 30 and 60 rpm were analyzed after exposing cells for 1 and 4 hours. For 75 rpm, cells were exposed for 1, 4 and 8 hours. After clinorotation was stopped, cell area and shape factor were analyzed every 30 min for 4 hours.

Table 1. Previously reported studies on mesenchymal stem cells under simulated microgravity.

Type of MSCs	Experimental device	Angular frequency	Duration	Results	Ref
Rat Bone marrow	Mitsubishi 3D Clinostat	**5 rpm**	12 hours	Decrease in alkaline phosphatase (marker of osteoblastic differentiation)	(43)
Human adipose derived	Rotatory bioreactor	**11-25 rpm**	21 days	**Microgravity promotes chondrogenesis via p38 MAPK pathway*** **	(21)
Rabbit Bone Marrow	Rotatory bioreactor	**20 rpm**	14 days	Microgravity promoted expression of collagen type II and Aggrecan	(44)
Human Bone Marrow	Rotatory bioreactor	**16 rpm**	7 days	**Decreased chondrogenic and osteogenic gene expression and increase adipogenic gene expression*** **	(22)
Rat Bone Marrow	2D Clinostat	**30 rpm**	72 hours	Endothelial differentiation potential was improved under microgravity	(45)
Human adipose derived	1D Clinostat	**15 rpm**	1 to 12 days	Ultrasound stimulation enhances osteogenic differentiation in microgravity	(46)
Human Bone Marrow	Rotatory Bioreactor	**	7 days	Increased the expression of PPARγ2, receptor important for adipogenesis	(47)
Human Bone Marrow	Rotatory Bioreactor	**9 rpm**	7 days	Microgravity affects integrin signaling and stress fibers, likely mediated by RhoA	(48)
Human Bone Marrow	Rotatory Bioreactor	**	7 days	Microgravity disrupts integrin/MAPK signaling	(49)
Rat Bone Marrow	2D Clinostat	**30 rpm**	3 days	Microgravity enhances differentiation into neurons with more mature action potentials	(50)
Rat Bone Marrow	2D Clinostat	**30 rpm**	24-96 hours	**Microgravity inhibits proliferation and osteogenesis*** **	(20)
Human Bone Marrow	3D Clinostat	**5 rpm**	2-4 weeks	**Microgravity stimulates proliferation (13-fold) and cells can still differentiate after exposure to microgravity*** **	(17)

** Indicates research that did not indicate a fixed rotation speed, since rotation speed was varied to prevent sedimentation. *** Notable contradictory findings.

Table 2. Number of cells measured for each condition in each experiment.

Cell Spreading Experiments									
Time (Hours)	0	1	2	3	4	5	6	7	8
NE=6									
0 rpm	30	31	30	45	44	60	37	31	31
30 rpm	30	31	49	47	48	44	40	36	37
60 rpm	30	51	57	60	60	55	58	47	50
75 rpm	30	31	30	32	45	33	36	32	36

Cell Morphology Experiments (Circularity)			
Time (Hours)	1	4	8
NE=3			
0 rpm	20	19	20
30 rpm	20	20	20
60 rpm	20	20	20
75 rpm	20	21	20

Cell Chemotaxis Experiments		
	Retraction	Migration
NE=3		
0 rpm		15
30 rpm	28	
75 rpm	28	6

Cell recovery after clinorotation	
0 rpm	9
30 rpm	9
60 rpm	9
75 rpm	12

Cell Viability Experiments			
Time (Hours)	1	4	8
0 rpm	30 Live/ 3 Dead	29 Live/ 4 Dead	28 Live/ 5 Dead
75 rpm	48 Live/ 5 Dead	47 Live/ 6 Dead	45 Live/ 8 Dead

NE indicates the number of independent experimental replicates.

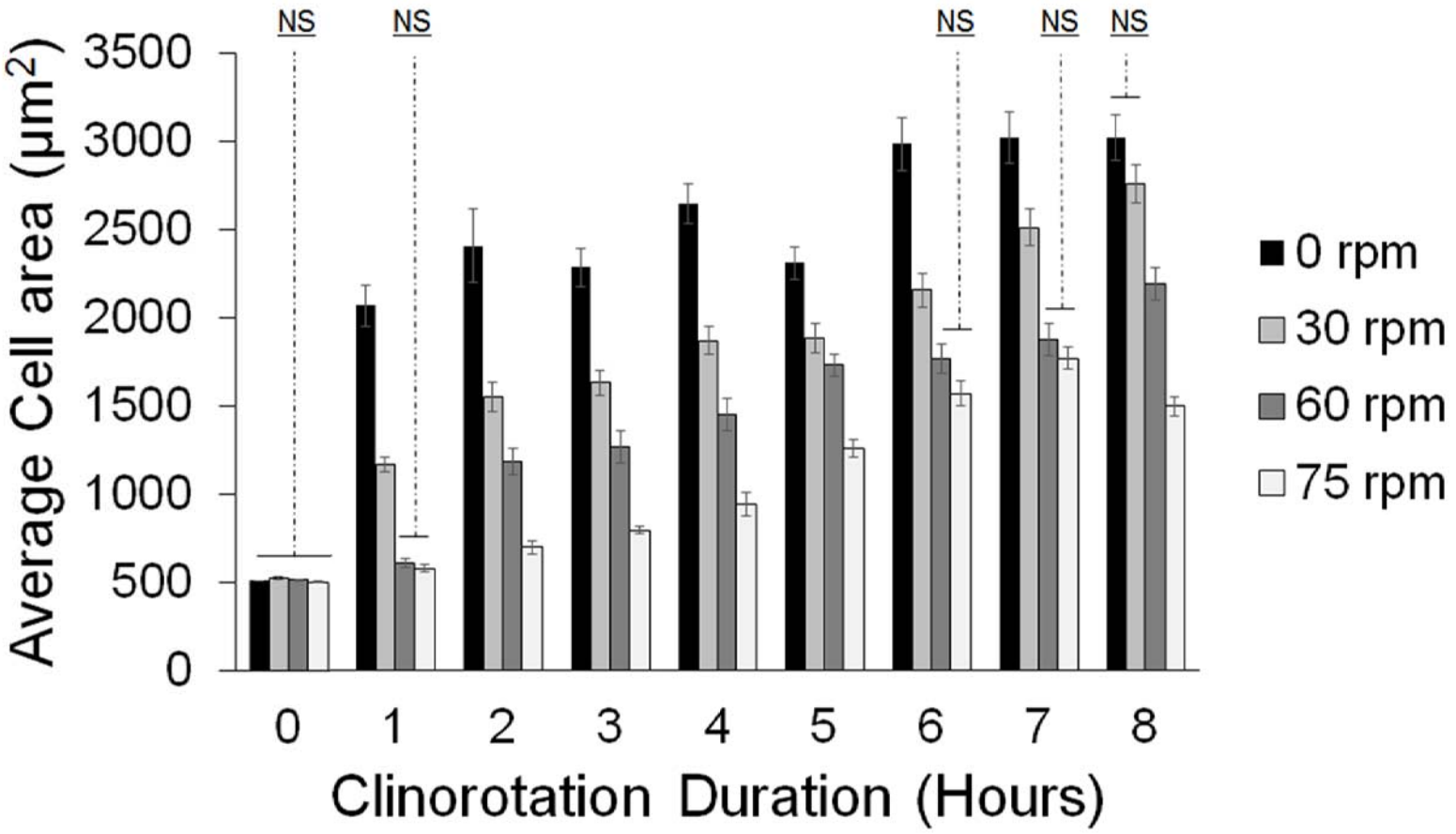
NS
NS
NS
NS
NS
Average Cell area (µm²)
3500
3000
2500
2000
1500
1000
500
0
0 rpm
30 rpm
60 rpm
75 rpm
0
1
2
3
4
5
6
7
8
Clinorotation Duration (Hours)

a)

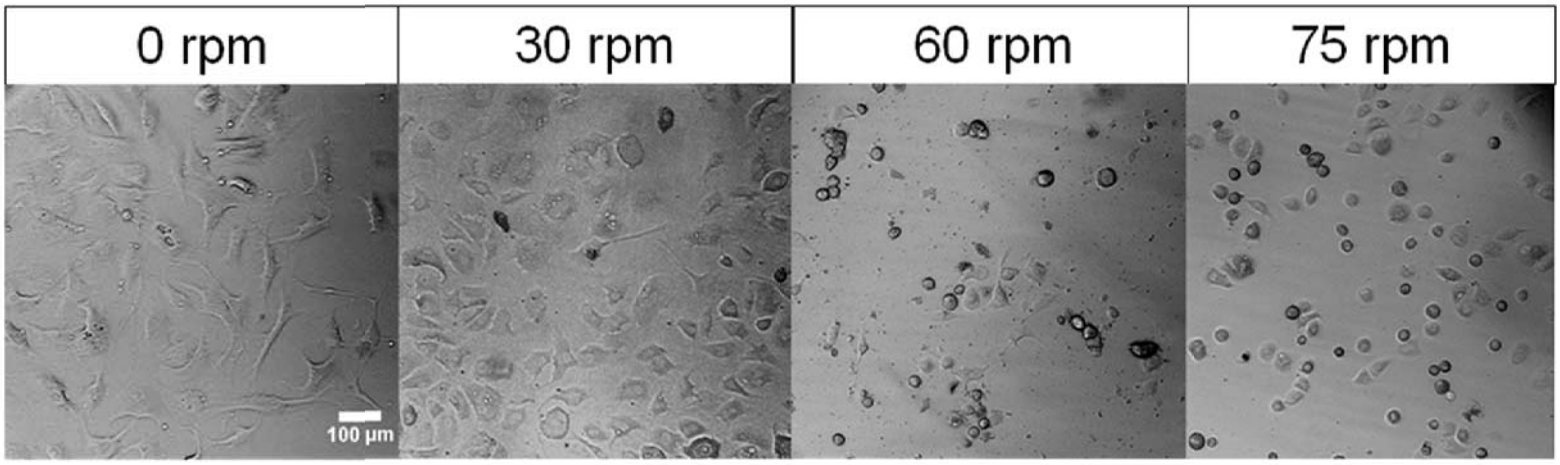
0 rpm
30 rpm
60 rpm
75 rpm
100 µm

b)

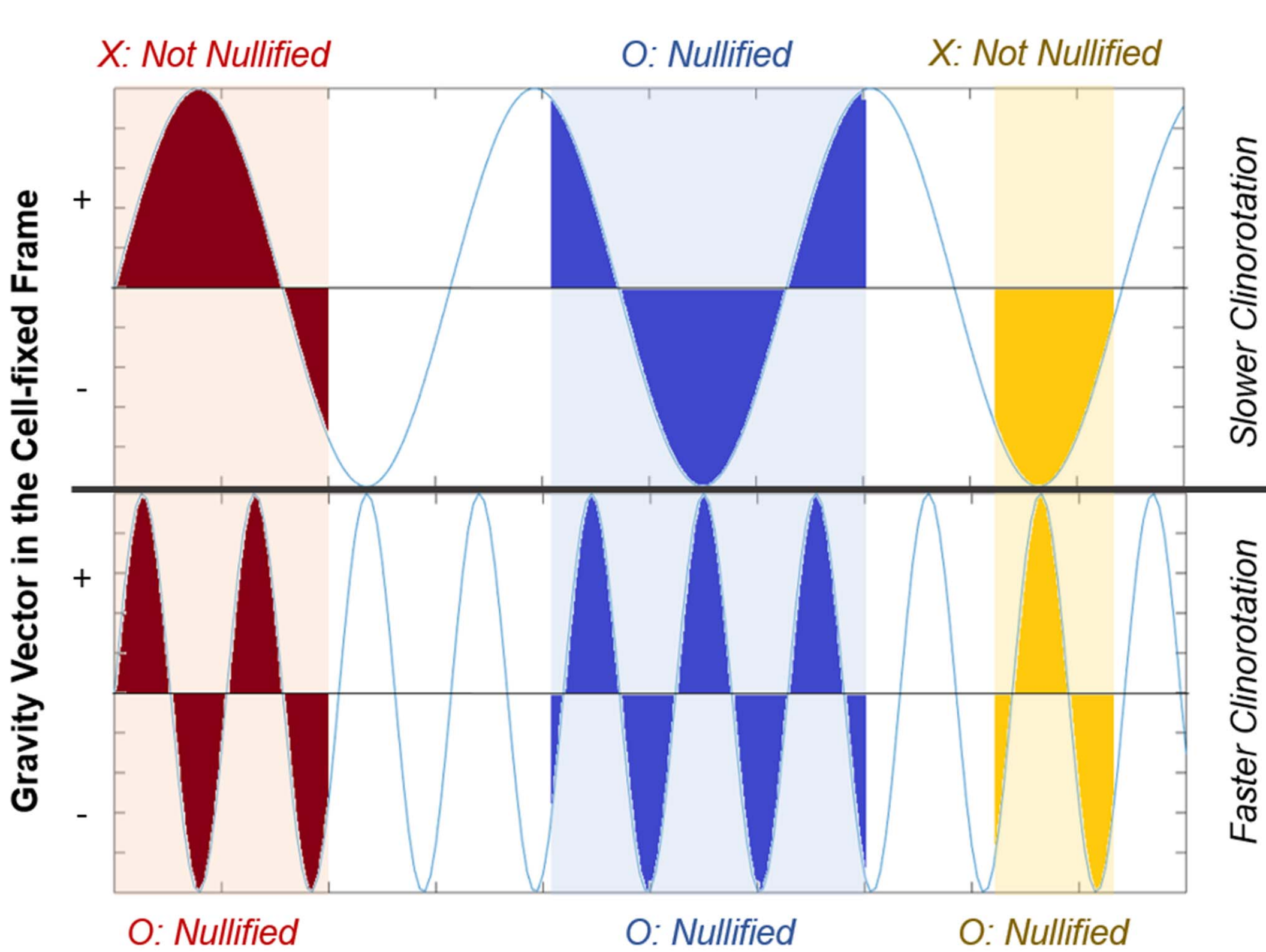
X: Not Nullified
O: Nullified
X: Not Nullified
Gravity Vector in the Cell-fixed Frame
+
-
Slower Clinorotation
+
-
Faster Clinorotation
O: Nullified
O: Nullified
O: Nullified

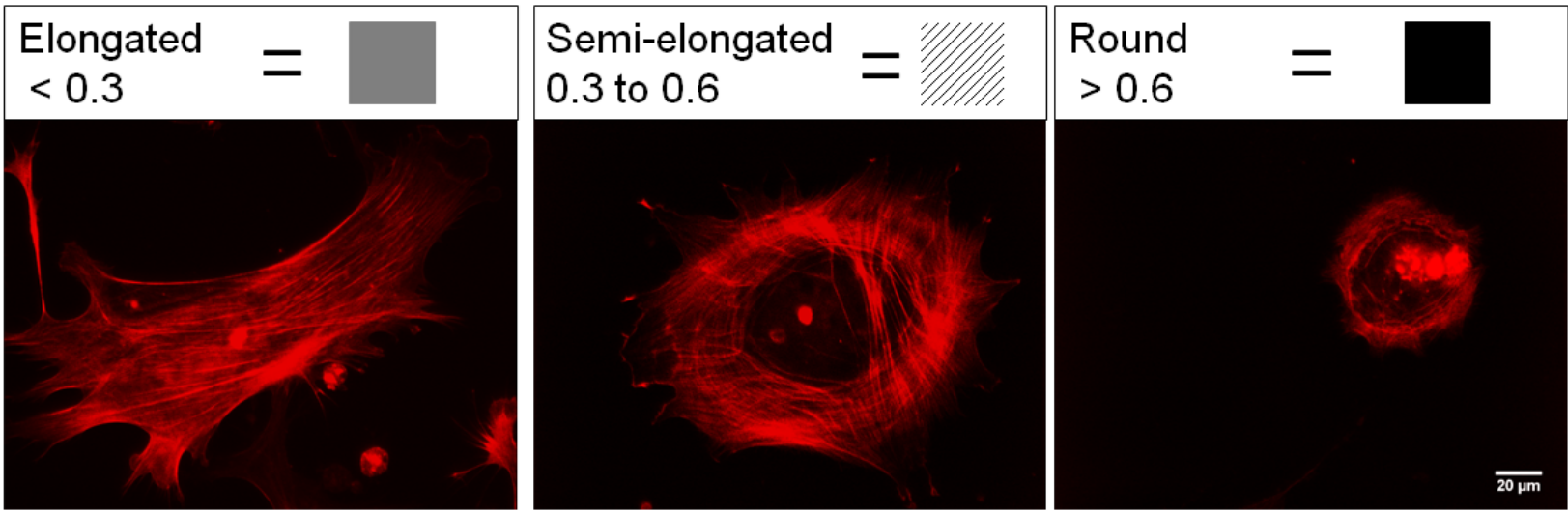
Elongated
< 0.3
Semi-elongated
0.3 to 0.6
Round
> 0.6
20 µm

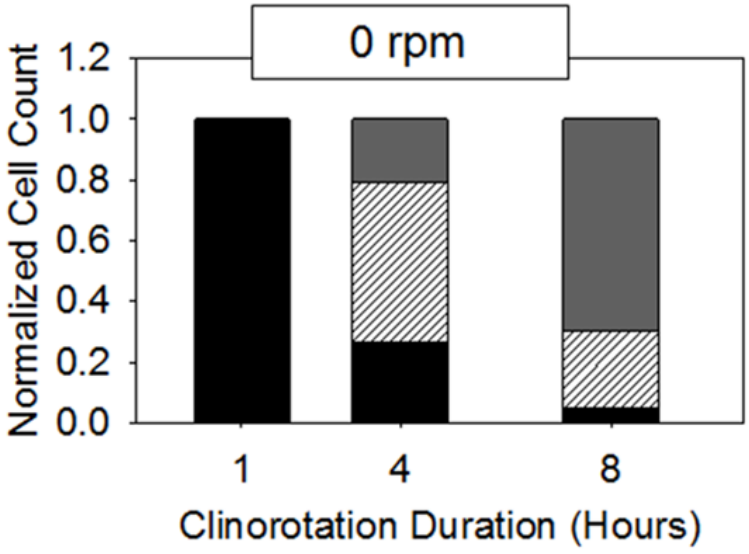
0 rpm
Normalized Cell Count
1.2
1.0
0.8
0.6
0.4
0.2
0.0
1
4
8
Clinorotation Duration (Hours)

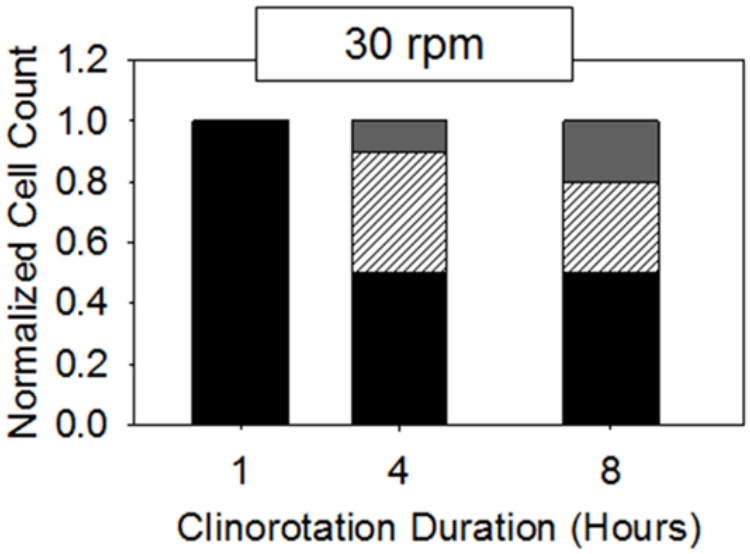
30 rpm
Normalized Cell Count
1.2
1.0
0.8
0.6
0.4
0.2
0.0
1
4
8
Clinorotation Duration (Hours)

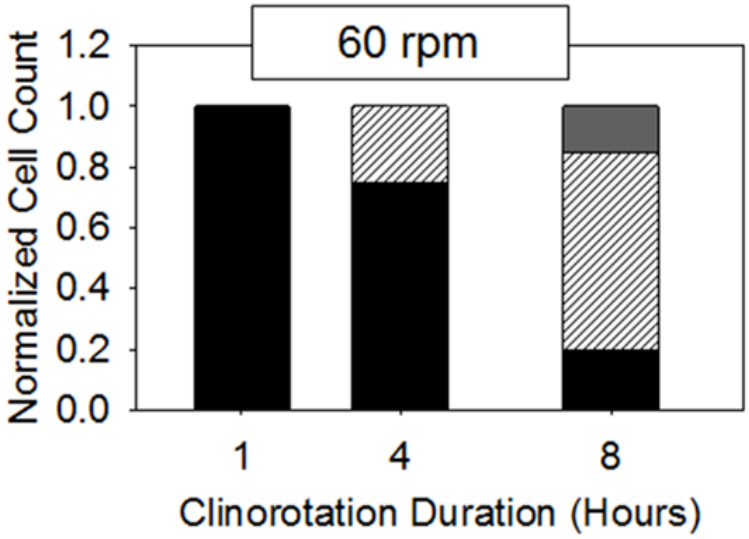
60 rpm
Normalized Cell Count
1.2
1.0
0.8
0.6
0.4
0.2
0.0
1
4
8
Clinorotation Duration (Hours)

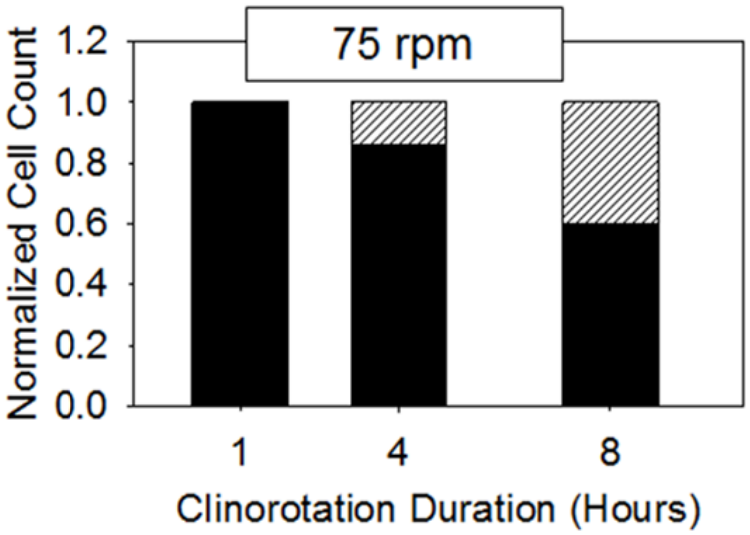
75 rpm
Normalized Cell Count
1.2
1.0
0.8
0.6
0.4
0.2
0.0
1
4
8
Clinorotation Duration (Hours)

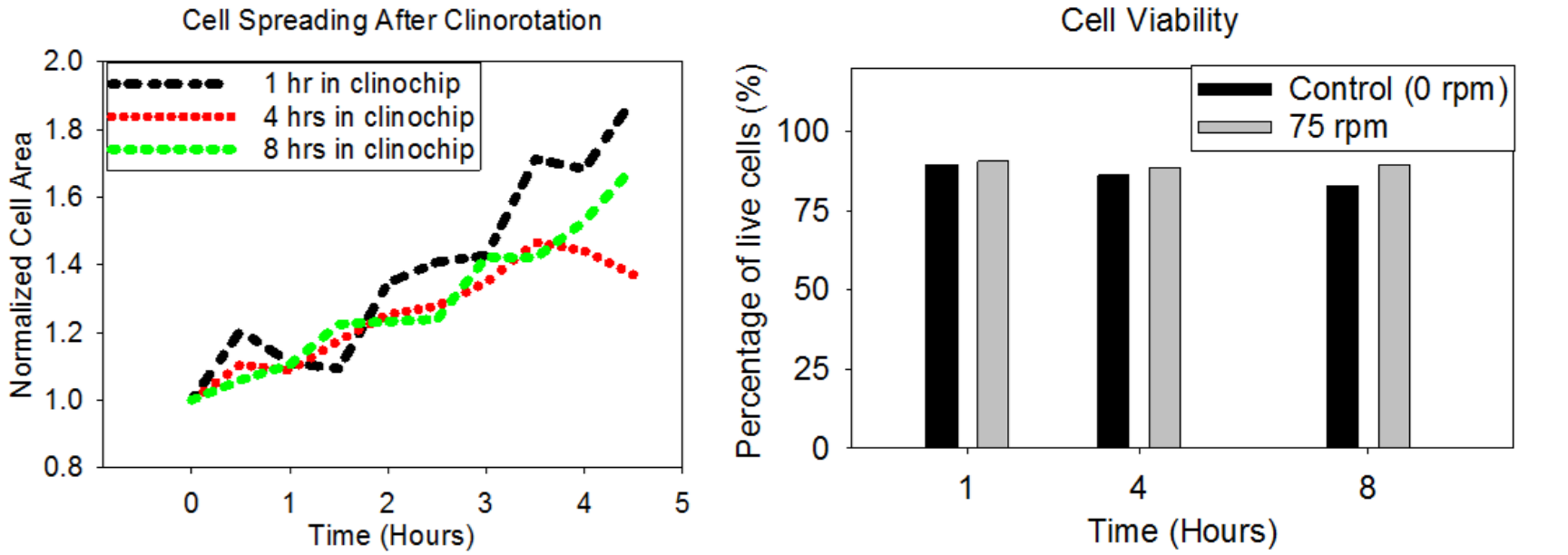

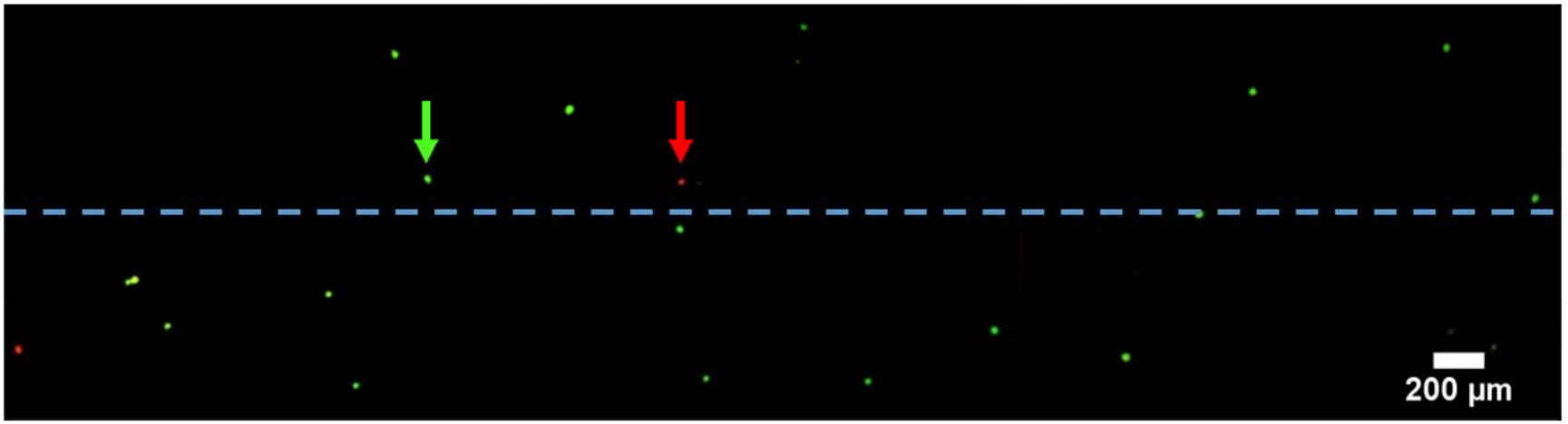

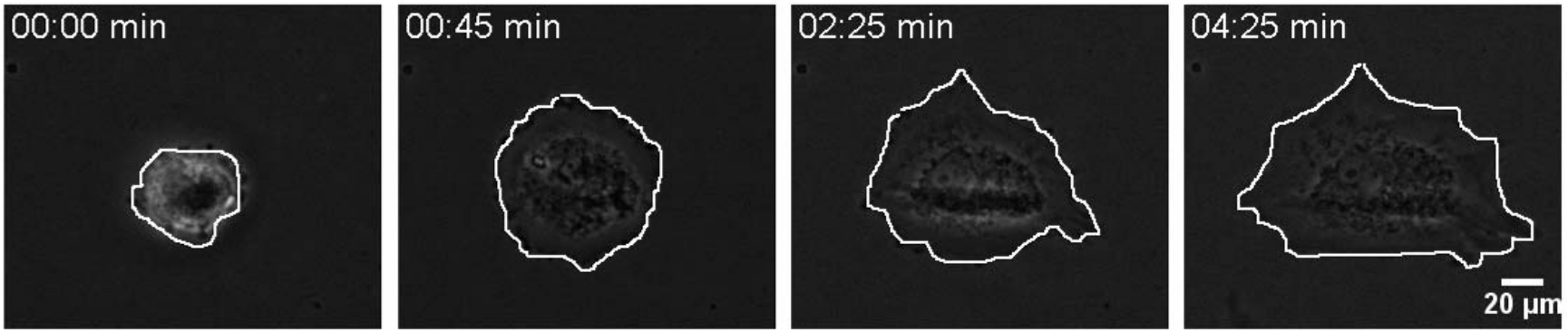

After clinorotation

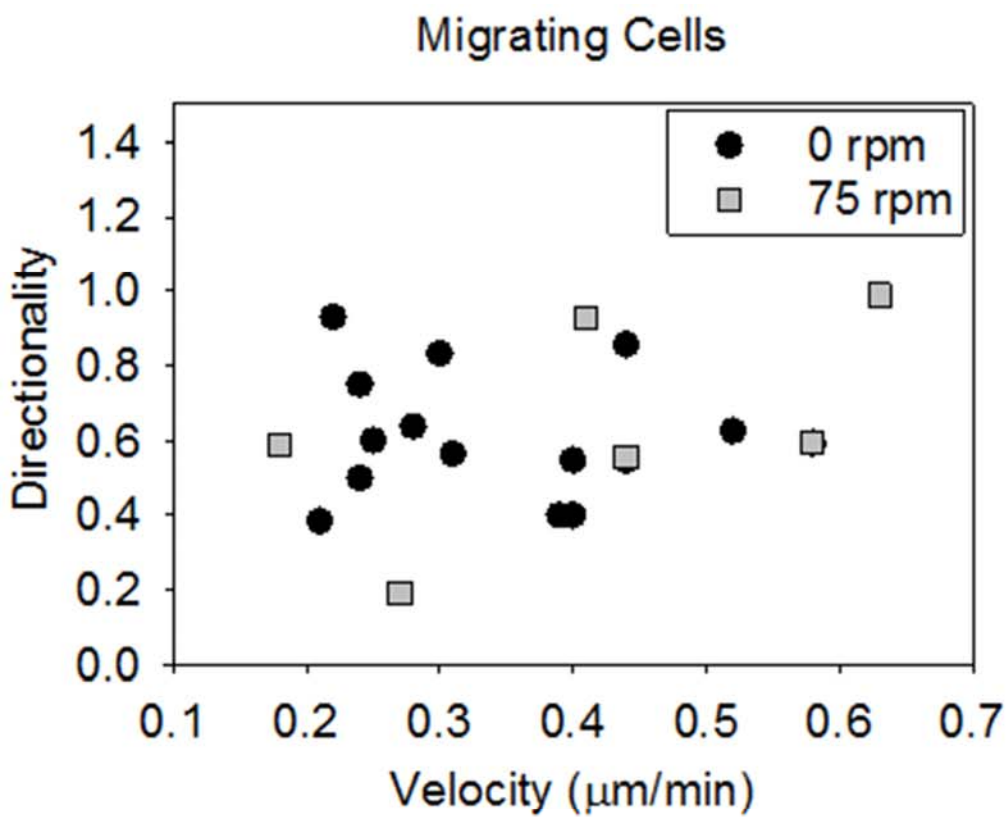
Migrating Cells
0 rpm
75 rpm
Directionality
1.4
1.2
1.0
0.8
0.6
0.4
0.2
0.0
0.1
0.2
0.3
0.4
0.5
0.6
0.7
Velocity (μm/min)

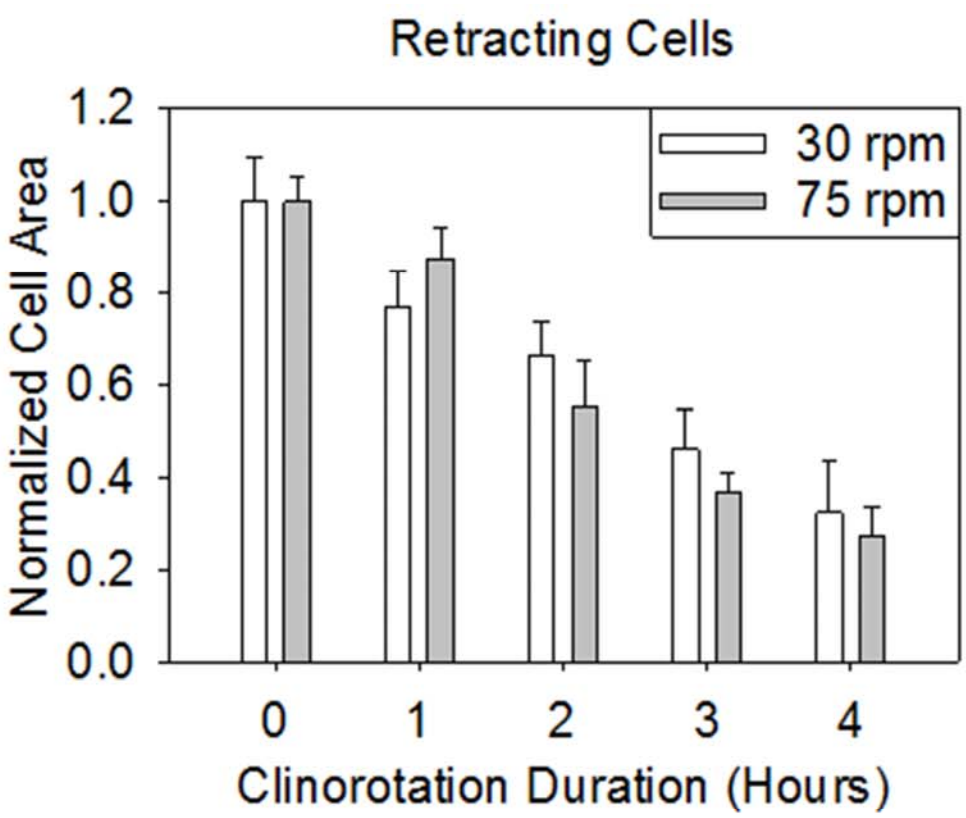
Retracting Cells
30 rpm
75 rpm
Normalized Cell Area
1.2
1.0
0.8
0.6
0.4
0.2
0.0
0
1
2
3
4
Clinorotation Duration (Hours)

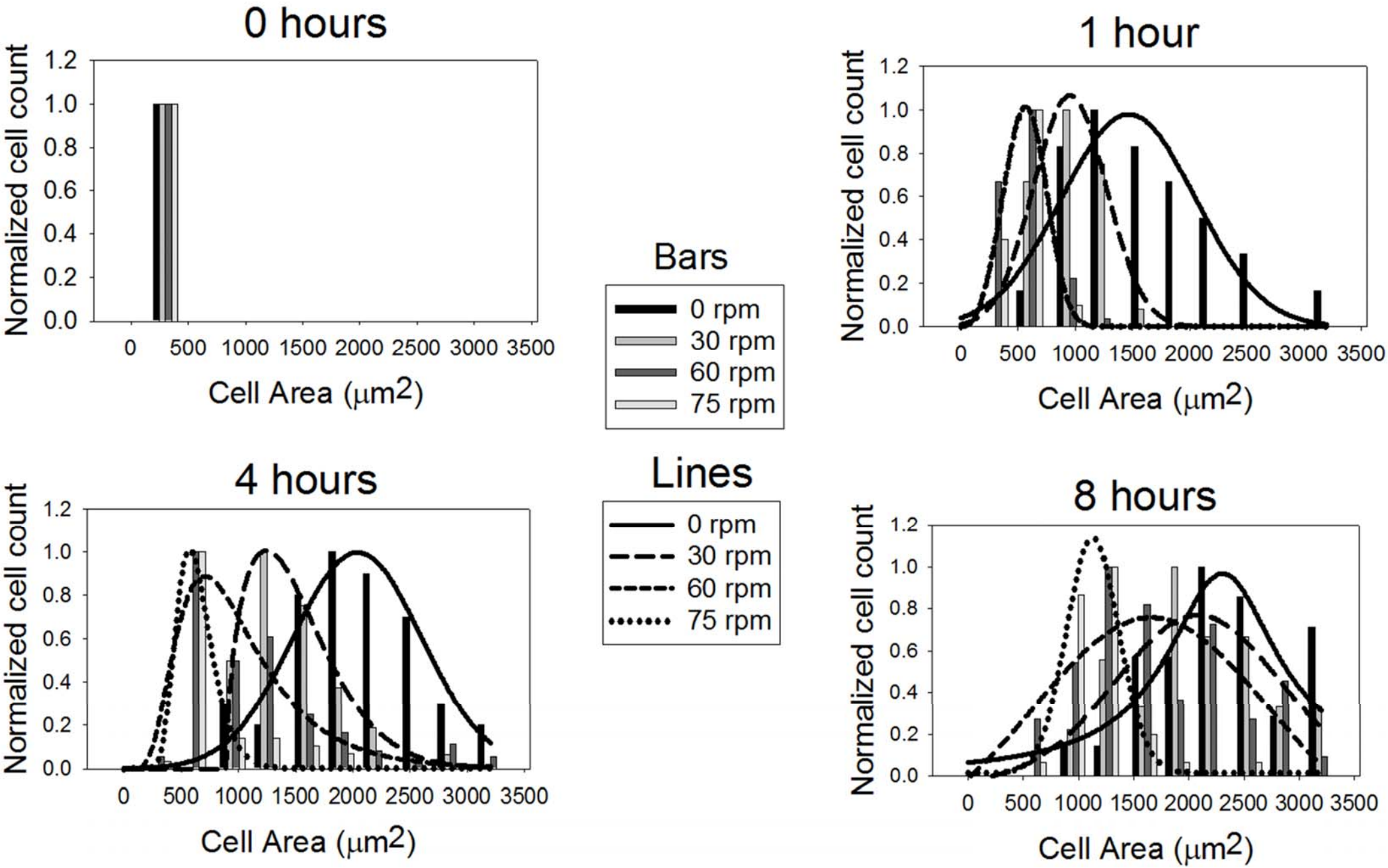
0 hours
1 hour
4 hours
8 hours
Normalized cell count
Cell Area (μm2)
0.0
0.2
0.4
0.6
0.8
1.0
1.2
0
500
1000
1500
2000
2500
3000
3500
Bars
0 rpm
30 rpm
60 rpm
75 rpm
Lines
0 rpm
30 rpm
60 rpm
75 rpm

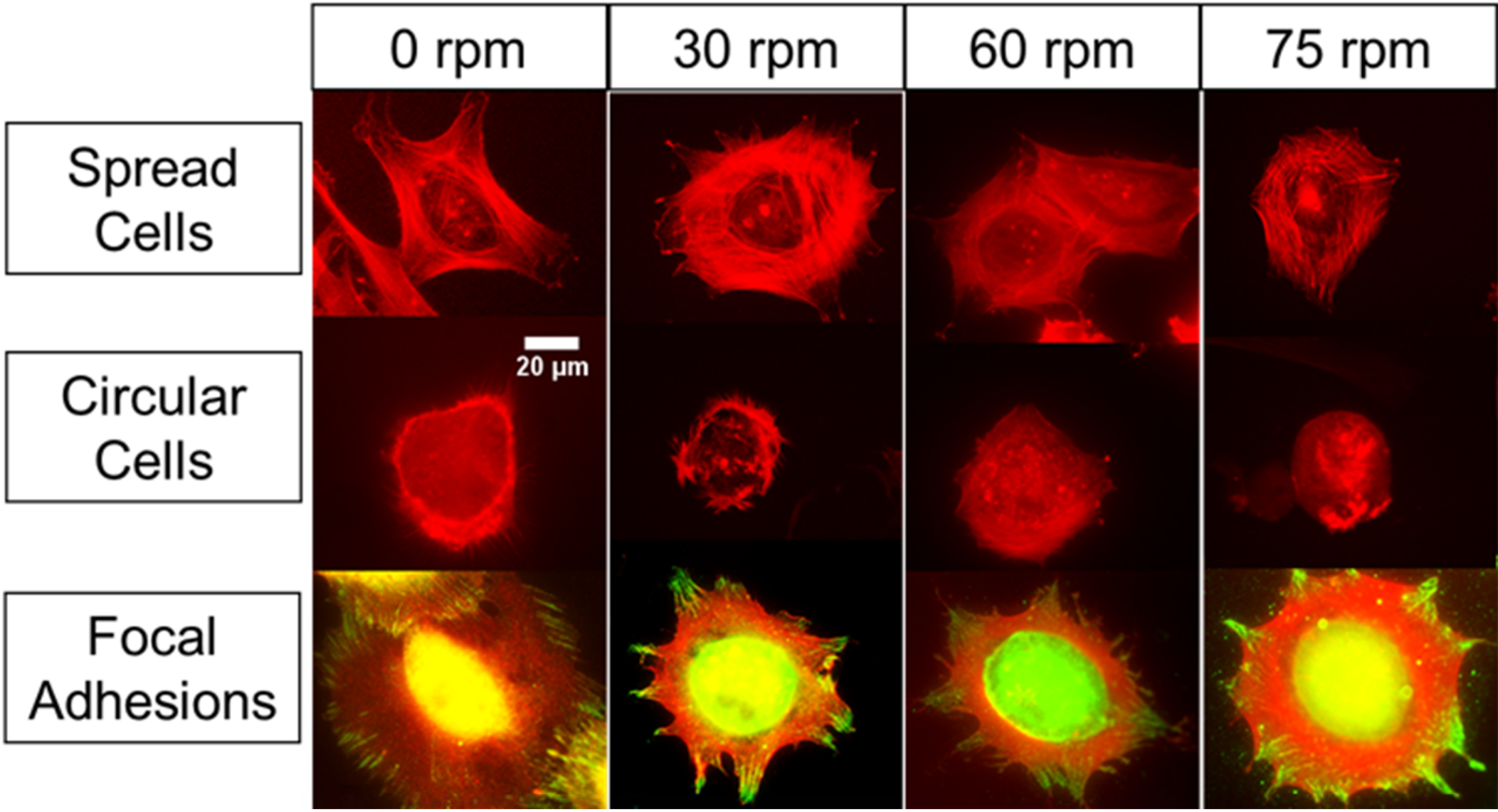
0 rpm
30 rpm
60 rpm
75 rpm
Spread Cells
Circular Cells
Focal Adhesions
20 µm

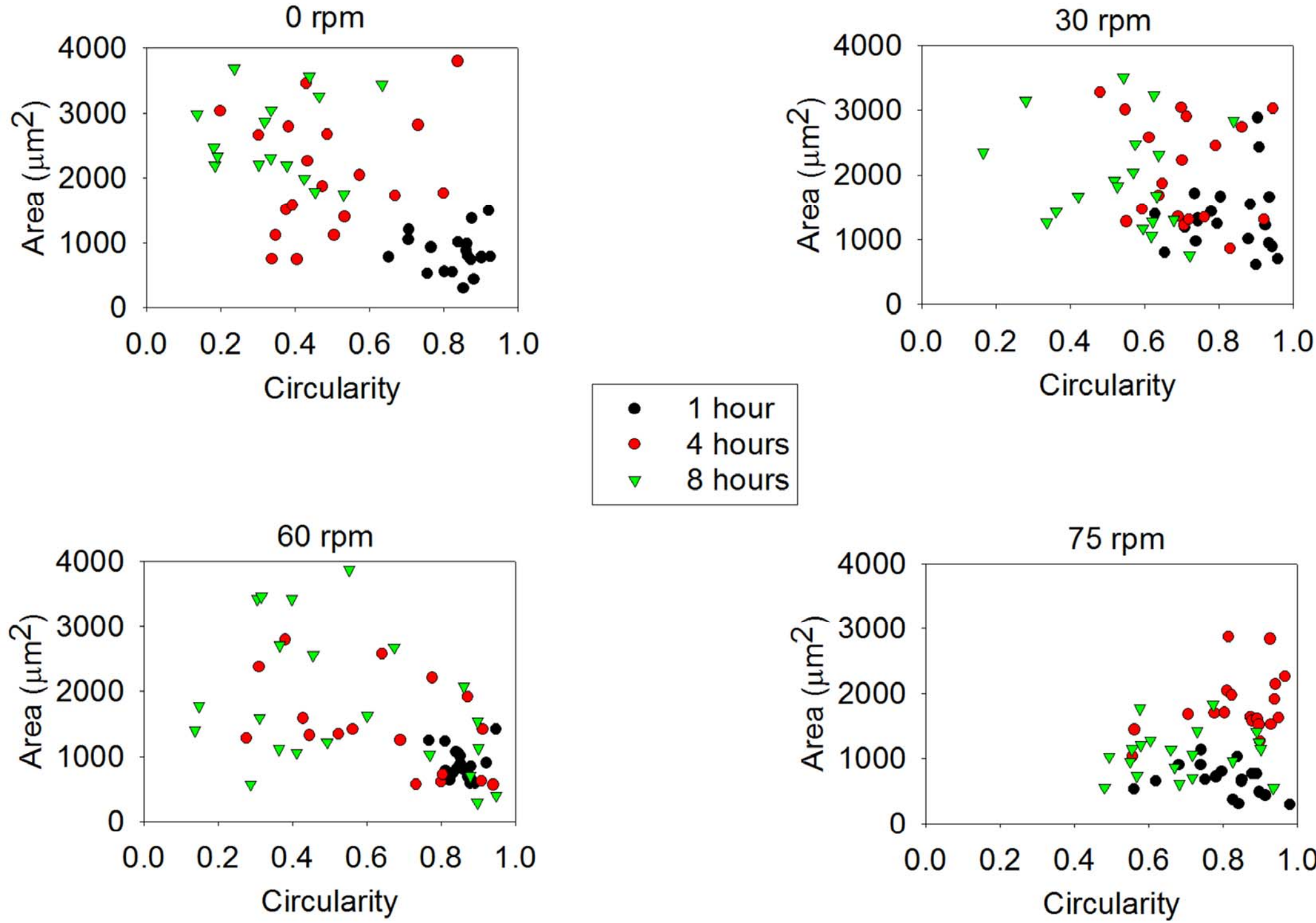
0 rpm
30 rpm
60 rpm
75 rpm
Area (µm2)
Circularity
0
1000
2000
3000
4000
0.0
0.2
0.4
0.6
0.8
1.0
1 hour
4 hours
8 hours

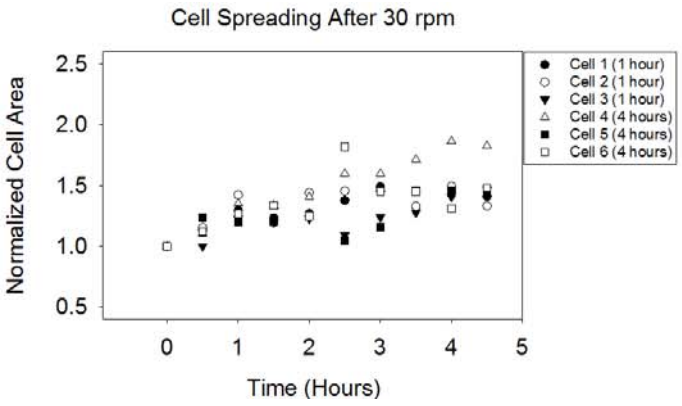
Cell Spreading After 30 rpm
Normalized Cell Area
Time (Hours)
Cell 1 (1 hour)
Cell 2 (1 hour)
Cell 3 (1 hour)
Cell 4 (4 hours)
Cell 5 (4 hours)
Cell 6 (4 hours)

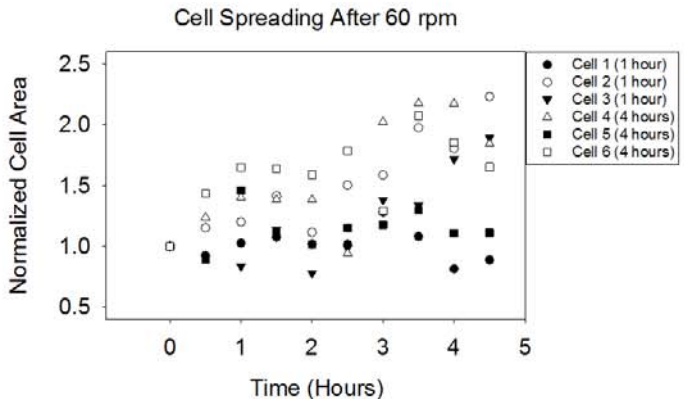
Cell Spreading After 60 rpm
Normalized Cell Area
Time (Hours)
Cell 1 (1 hour)
Cell 2 (1 hour)
Cell 3 (1 hour)
Cell 4 (4 hours)
Cell 5 (4 hours)
Cell 6 (4 hours)

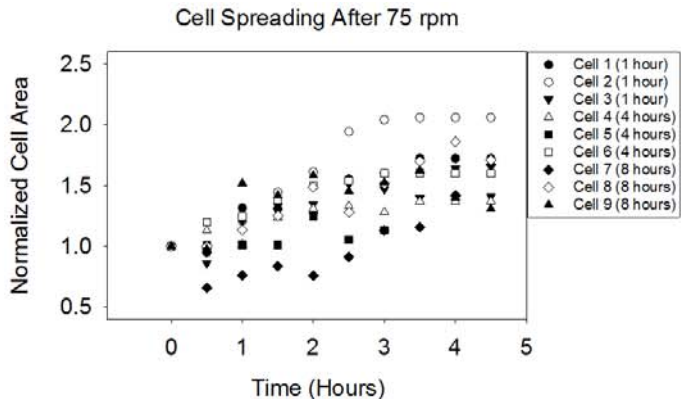
Cell Spreading After 75 rpm
Normalized Cell Area
Time (Hours)
Cell 1 (1 hour)
Cell 2 (1 hour)
Cell 3 (1 hour)
Cell 4 (4 hours)
Cell 5 (4 hours)
Cell 6 (4 hours)
Cell 7 (8 hours)
Cell 8 (8 hours)
Cell 9 (8 hours)

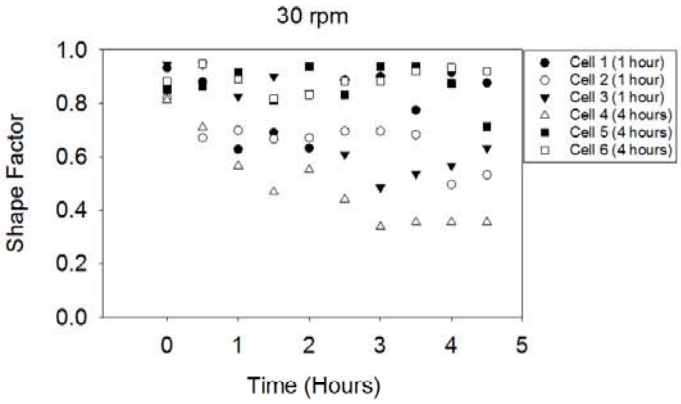
30 rpm
Shape Factor
Time (Hours)
Cell 1 (1 hour)
Cell 2 (1 hour)
Cell 3 (1 hour)
Cell 4 (4 hours)
Cell 5 (4 hours)
Cell 6 (4 hours)

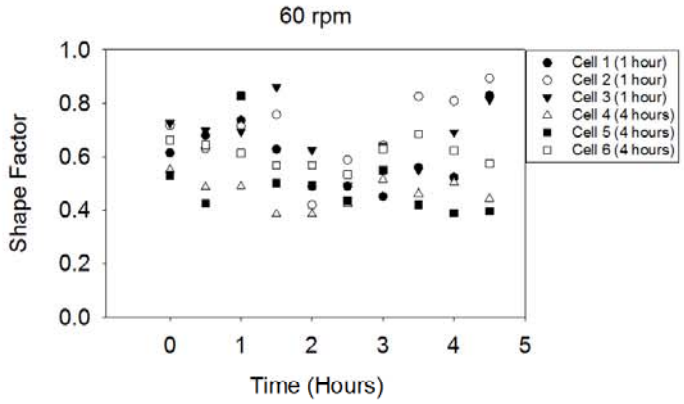
60 rpm
Shape Factor
Time (Hours)
Cell 1 (1 hour)
Cell 2 (1 hour)
Cell 3 (1 hour)
Cell 4 (4 hours)
Cell 5 (4 hours)
Cell 6 (4 hours)

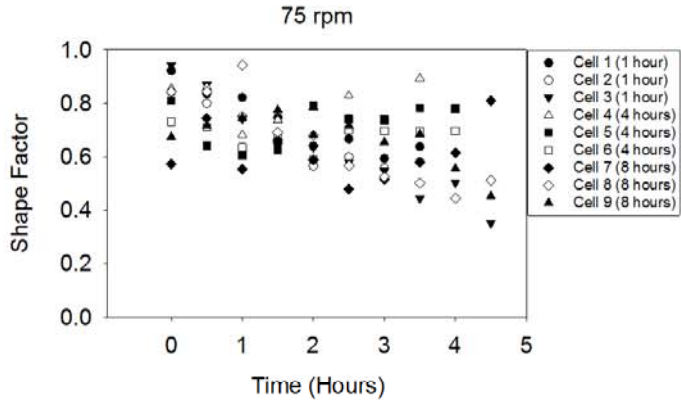
75 rpm
Shape Factor
Time (Hours)
Cell 1 (1 hour)
Cell 2 (1 hour)
Cell 3 (1 hour)
Cell 4 (4 hours)
Cell 5 (4 hours)
Cell 6 (4 hours)
Cell 7 (8 hours)
Cell 8 (8 hours)
Cell 9 (8 hours)